

Laser driven Secondary Photon emission by Silicon Photomultipliers

Priyanka Kachru^{a,*}

^a*Department of Physics, University of Massachusetts Amherst,
710 North Pleasant Street Amherst, MA 01003, USA*

E-mail: pkachru@umass.edu

Secondary photons in SiPMs are responsible for at least three processes: (i) internal cross-talk (ii) external cross-talk and (iii) optically-induced afterpulsing. While the internal crosstalk and afterpulsing involves photon transport within the SiPM, the external cross-talk photons escape from the surface of one SPAD and potentially: (i) reflect back into the SiPM at the surface coating interface and trigger avalanches in neighbouring SPADs, (ii) transmit through the SiPM surface coating. Since some of the future multi-ton dark matter and neutrinoless double beta decay experiments are choosing SiPMs as photosensors, the external crosstalk can be a significant background due to each SiPM's tendency to trigger a nearby one. This mechanism may cause detector background and reduce the accuracy of photo-electron resolution for high photo-electron events, leading to a degradation in the position and energy reconstruction.

To quantify the systematic effects which deteriorate the overall performance of such detectors, a study on SiPM secondary photon emission was conducted. The SiPMs tested were 1 cm² FBK NUV HD-cryo. It determined the absolute secondary photon yield equal to the number of photons emitted per charge carrier (γ/e^-) using spectroscopy. The photon yields were calculated at 163 K and 87 K to mimic the SiPM performance at liquid Xenon (LXe) and liquid Argon (LAr) temperatures. A summary of the spectroscopy technique and data analysis used to quantify the secondary photon yield at cryogenic temperatures is reported.

*XVII International Conference on Topics in Astroparticle and Underground Physics (TAUP 2023)
28 August - 1 September 2023
University of Vienna, Austria*

*Speaker

1. Introduction

The secondary photon emission in silicon is summarised with a combination of three mechanisms at play [2]: (i) indirect interband transitions, (ii) intraband Bremsstrahlung processes and (iii) direct interband transitions [2–4]. Each of these mechanisms corresponds to specific wavelength regions. Fig. 1 (right) encapsulates the above mechanisms corresponding to the spectral regions.

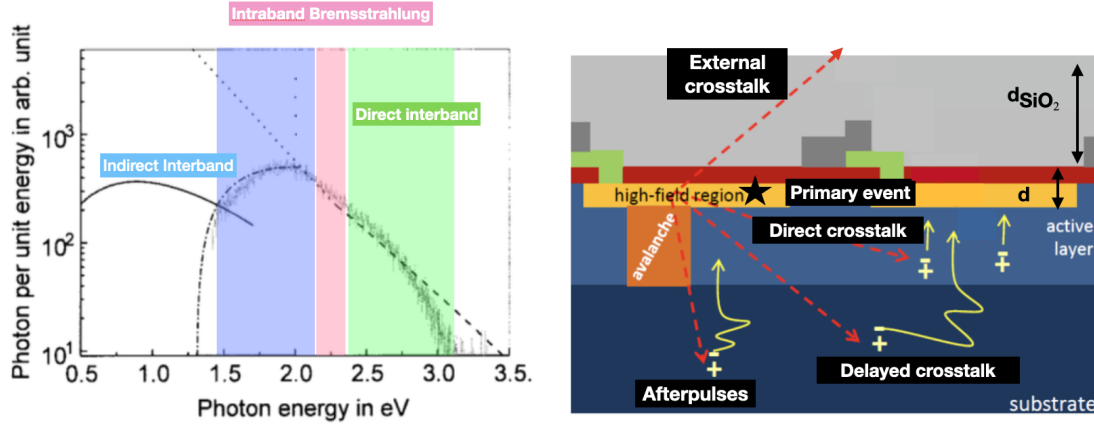


Figure 1: **Left:** The multimechanism model for silicon p-n junction diode describing different parts of spectrum [3]. **Right:** The cross-sectional of the SiPM showing the primary event occurring and leading to various isotropic emission of SiPM noises. The d_{SiO_2} and d are the depths of the SiO_2 coating on the SiPM and the depth of the depletion region respectively.

Silicon Photomultipliers (SiPMs) are Solid-state semiconductor devices used as photo-detectors in modern experiments and are based on the physics of reverse biased p-n junction diodes. Fig. 1 (left) shows the cross-sectional view of the SiPM showing the various noises that it generates isotropically. SiPM noises have been discussed in detail in many literatures [5–7]. External crosstalk is the secondary photon emission phenomenon where generated photons escape the SiPM surface triggering the neighbouring SiPMs. This could degrade the energy resolution and position reconstruction of keV-scale events resulting from inaccurate photo-electron resolution. The future SiPM-based low-energy particle physics experiments will have to study and quantify the effect of external crosstalk to determine the sensitivity of their experiments [8, 9].

2. Experimental Setup

A dedicated hardware setup was developed at TRIUMF Canada to study the SiPM photon emission as a function of the applied over voltage and temperature. It consists of a vacuum cryostat chamber mounted on top of an Olympus IX83 microscope. Inside the chamber, the SiPM with its electronics is affixed to a translation stage, facing down towards the microscope with sub-micron motorized position adjustment in the XY-plane as shown in Fig. 2 (left). The light emitted from the SiPM is collected in Princeton Instruments (PI) PyLoN[®]400BR_eXcelon CCD camera which is used with a Princeton Instruments HRS 300-MS Spectrometer.

Earlier studies performed with this setup were used to characterize photon emission as a result of dark noise-driven avalanches at room temperature, at high over-voltages ($> 8 V_{OV}$), to acquire

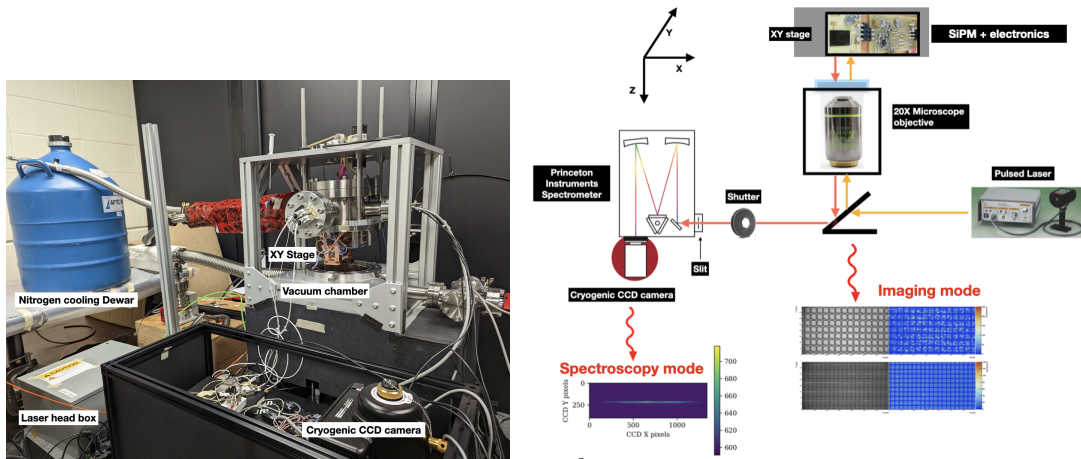


Figure 2: **Left:** Complete hardware setup with its cooling stage, XY stage position and cryogenic CCD camera. **Right:** The optical system used for the SiPM photon emission spectroscopy. It contains the SiPM + its electronics on the XY motorized stage facing down, towards the microscope objective preceded by a Sapphire window. Other elements such as a dichroic mirror, a long pass filter, a pulsed laser and the spectrometer attached to the cryogenic CCD camera are also shown.

good statistics as shown in Ref. [10]. The laser injection system used for this study is shown in Fig. 2 (right), which allows SiPM to be operated at OVs nominal for future dark matter and neutrinoless double decay experiments. It comprises of several components: (i) a Picoquant laser (405 nm) to provide a picosecond pulsed illumination to the SiPM. (ii) LUCPLFLN20X microscope objective optimized for transmission in the near-infrared wavelength range with a 20x magnification. (iii) Edmund optics dichroic mirror with a cutoff wavelength of 550 nm. (iv) A dichroic mirror is followed by an Edmund Optics 550 nm long pass filter.

The PI spectrometer is attached to the microscope via a C-mount adapter and it is equipped with a 150 lines/mm blazed diffraction gratings with peak efficiency at 800 nm and optimal transmission in the visible and near-infrared (NIR) wavelength range. Secondary photon emission in the UV and vacuum ultraviolet (VUV) is in fact expected to be low, as shown in previously reported measurements [11].

The pulsed laser illuminates a SPAD on the SiPM through the dichroic mirror and microscope. The laser-stimulated photons from the SPAD pass through the microscope and long pass filter : (i) to enter the spectrometer via a shutter and adjustable slit. It then undergoes diffraction to capture the spectral components at infrared wavelengths. This is the spectroscopy mode of the system. (ii) to enter a secondary camera for localising the laser spot onto the SPAD. Additionally, the PI spectrometer grating was set to its 0th-order. This is the imaging mode of the system.

3. Experimental results

3.1 Spectral analysis

The spectroscopy mode of the TRIUMF setup was used to measure the spectral shape of the secondary photon emission for the SiPM with the laser-focused on a SPAD. The 1 cm² FBK NUV

HD-Cryo SiPM was operated between 2-12 V_{ov} for 87 K and 163 K. The SiPM pulse counting data were recorded with a High Definition oscilloscope. Each recorded waveform was 10 μs long, with 5 μs of pre-trigger. The emission spectra were instead recorded with the PI LightField® software.

The net normalization from raw ADC Units (ADU)s recorded by the PI camera, $N_{\text{ADU}}^{\text{SPAD}}(\lambda)$, to the number of emitted photons (γ) observed per avalanche was obtained as follows [γ/av]

$$N_{\text{av}}(\lambda) = \frac{N_{\text{ADU}}^{\text{SPAD}}(\lambda) \eta_{\text{ADU}}^{\gamma}}{\mu_{\text{av-exp}}} \left(\frac{1}{\epsilon(\lambda)} \right) \quad (1)$$

where: $\eta_{\text{ADU}}^{\gamma}$ is the calibrated gain of the PI camera equal to 0.7 γ/ADU ¹; $\epsilon(\lambda)$ is the TRIUMF setup detection transmission efficiency, as shown in Fig. 6. $\mu_{\text{av-exp}}$ is instead the total number of avalanches produced by the laser in each exposure of time $\Delta t = 500$ s. This can be computed as follows: $\mu_{\text{av-exp}} = P_{\text{trig}}^{\text{av}} \times f \times \Delta t$. with f laser frequency equal to 125 kHz. $P_{\text{trig}}^{\text{av}}(V)$ is instead the probability of the selected SPAD firing. It can be measured by counting the number of laser flashes in which no pulses were detected (N_0) as follows: $P_{\text{trig}}^{\text{av}} = 1 - N_0/N_{\text{tot}}$.

Fig. 3 (left) shows that the observed photons per avalanche per nm increase with the over-voltage: $N_{\gamma}^*(\lambda)$, for the SiPM tested.

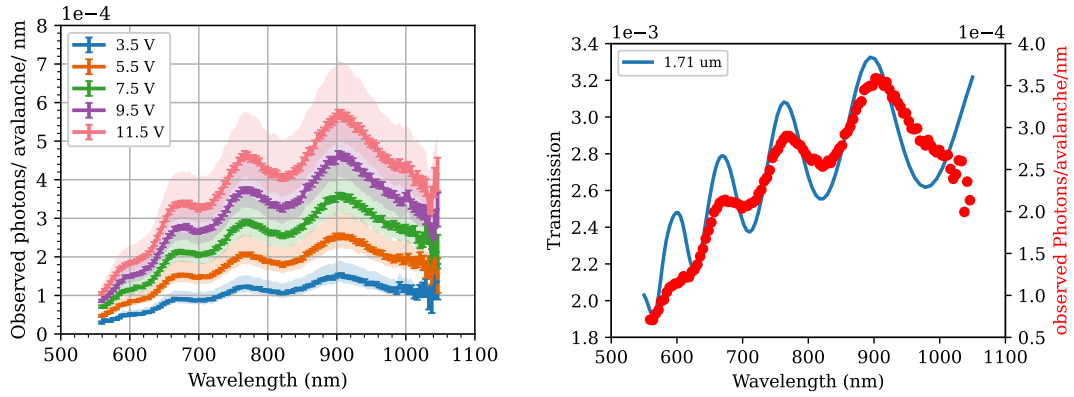


Figure 3: Left : Observed photon emission spectrum per avalanche per nm measured at different over-voltages for 87 K as a function of the wavelength. The shaded bands show the measurement of systematic uncertainty. **Right :** Simulated transmission (in blue) and observed photons per avalanche per nm (in red points) as a function of wavelength used to match the oscillation peaks originating from the interference of light with the SiO₂ surface coating structure on the SiPM. The transmission curve was simulated assuming the SiO₂ thickness as 1.71 μm.

It is defined as [$\gamma/(\text{av} \times \text{nm})$] as: $N_{\gamma}^*(\lambda) = N_{\text{av}}(\lambda)/\Delta\lambda$, where $\Delta\lambda$ represents the wavelength resolution, equal to 1.7 nm. The oscillations feature seen in the spectra comes from the interference of light with the silicon dioxide (SiO₂) thin-film coating on the surface of SiPM.

So far, the factor $N_{\text{av}}(\lambda)$ does not account for: (i) the finite numerical aperture (NA) of the microscope objectives lenses, (ii) reflection and absorption losses due to the SiPM surface coating and the depth to the location of the avalanche region. A correction factor $A(\lambda)$ can be applied to

¹The camera gain is the independent from the wavelength since it refers to the gain applied by the preamplifier inside the camera after the exposure time has elapsed.

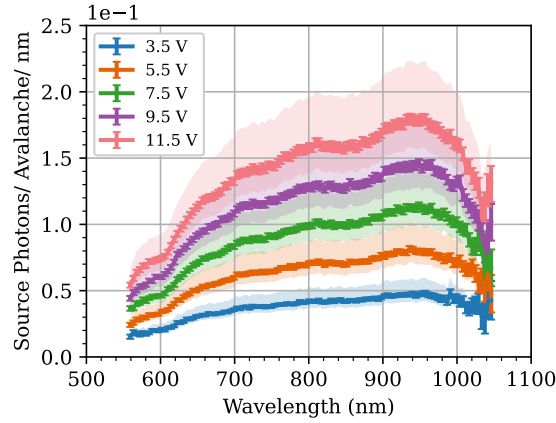


Figure 4: Inferred source photon emission per avalanche per nm at different overvoltages for 87 K as a function of the wavelength.

the data to obtain an estimation of the number of source photons per avalanche per nm produced in the SiPM as follows : $N_{av}^S(\lambda) = N_{av}(\lambda)/A(\lambda)$

Unfortunately, the correction factor $A(\lambda)$ cannot be precisely computed due to the unknown geometry and material of the SiPM anti-reflective coating structure. A raw estimate can be computed assuming a Silicon (Si) - SiO₂ interface, anti-reflective coating layer at the top of the SiPMs, as done in Ref. [13]. The estimation of the SiO₂ layer thickness was done by trying to match the peaks of the oscillations as shown in Fig. 3 (right). The simulation assumed the thickness of the SiO₂ layer as 1.71 μm .

The Lumerical 3D simulation software [14] was then used to extrapolate the $A(\lambda)$ factor and to obtain the number of source photons per avalanche per nm, defined as:

$$N_{\gamma}^{S*}(\lambda) = \frac{N_{av}^S(\lambda)}{\Delta\lambda} \quad (2)$$

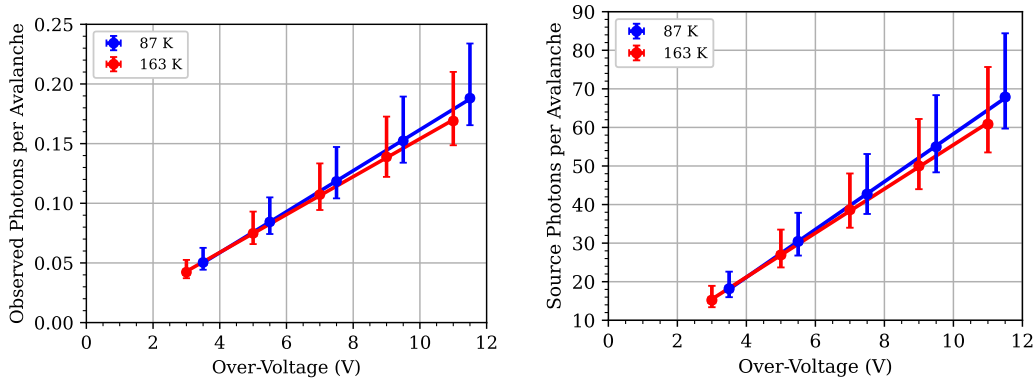


Figure 5: Observed and inferred source photons per avalanche integrated over the emission spectrum at 87 K and 163 K.

Fig. 4 shows source photons per avalanche per nm with no oscillation pattern after applying the source correction factor from Lumerical. Fig. 5 (left) shows the integrated observed photons

per avalanche over range of wavelengths (560 nm - 1050 nm) and Fig. 5 (right) shows the source photons per avalanche produced in the SiPM. The best estimate of the system's photon acceptance is found to be 0.4% due to the microscope's numerical aperture, resulting in a loss of 99.6% of source photons. This is because photons are produced isotropically at the emission source, but only a fraction that falls within the numerical aperture of the microscope is observed.

4. Conclusion

A study on secondary photon emission was done to extrapolate the systematic effect that could deteriorate the detector performance. The observed and source number of photons per avalanche were quantified at optimal voltages following the operation of future LXe or LAr-based experiments. There was no temperature dependence observed. The observed number of photons was found to be only 0.4% of the source photons produced isotropically in the SiPM. The observed photons per avalanche ranged from 0.05 - 0.2 and source photons per avalanche ranged from 15 - 65 for 2 - 12 V_{OV} . The next steps for this study would include extrapolating the observed emission spectra in different experimental media like LAr and LXe. This will precisely determine the amount of light produced by one SiPM in a detector medium that can propagate to other SiPMs of the detector.

5. Acknowledgments

I would like to acknowledge support from the Istituto Nazionale di Fisica Nucleare (Italy) and Laboratori Nazionali del Gran Sasso (Italy), from NSF (US, Grant PHY-1622415 and PHY-1812540 for Princeton University, USA), and the European Union's Horizon 2020 research and innovation programme under DarkWave project.

References

- [1] R. Newman, (1955), *Visible Light from a Silicon p-n Junction*, doi:10.1103/PhysRev.100.700, Physical Review, volume 100.
- [2] Lacaita, A.L. and et al., (1993), *On the bremsstrahlung origin of hot-carrier-induced photons in silicon devices*, doi: 10.1109/16.199363, IEEE Transactions on Electron Devices, volume 40.
- [3] Akil, N. and et al., (1999), *A multimechanism model for photon generation by silicon junctions in avalanche breakdown*, doi: 10.1109/16.760412, Electron Devices IEEE Transactions, volume 46.
- [4] Gautam, DK. and et al., (1988), *Photon emission from reverse-biased silicon PN junctions*, Solid-state electronics- Elsevier, volume 31.
- [5] S. Gundacker and A. Heering. *The silicon photomultiplier: fundamentals and applications of a modern solid-state photon detector*. Physics in Medicine & Biology, 65(17):17TR01, 2020.
- [6] S.M.Sze. *Physics of Semiconductor Devices* Physics of Semiconductor Devices, volume 10. 1995.

- [7] F. Acerbi and et al. Understanding and simulating sipms. Nuclear Instruments and Methods in Physics Research Section A, 926:16–35, 5 2019.
- [8] S. Al Kharusi et.al., (2018), *nEXO pre-Conceptual Design Report*, <https://arxiv.org/pdf/1805.11142.pdf>.
- [9] C. E. Aalseth et.al., (2018), *Darkside-20k: A 20 tonne two-phase lar tpc for direct dark matter detection at lngs*, The European Physical Journal Plus, 133:131.
- [10] J. B. McLaughlin and et al., (2021), *Characterisation of SiPM Photon Emission in the Dark.*, Sensors, 21(17):5947.
- [11] R. Mirzoyan and et al., (2009), *Light emission in si avalanches.*, Nuclear Instruments and Methods in Physics Research Section A, 610(1):98–100.
- [12] A Halma Company. *Halogen calibrated light sources installation and operation manual.*, <https://www.oceaninsight.com/globalassets/catalog-blocks-and-images/manuals--instruction-ocean-optics/radiometrically-calibrated-ls/hl3pluscal1.pdf>.
- [13] G. Gallina and et al. (2019), *Characterization of sipm avalanche triggering probabilities.*, IEEE Transactions on Electron Devices, 66:4228–4234.
- [14] Ansys lumerical fdtd simulation for photonic components., <https://www.ansys.com/products/photonics/fdtd>.

A. Appendix

A.1 Intensity calibration

The intensity calibration of the entire setup is done by estimating a transmission intensity curve. The modelled transmission intensity is the product of transmission efficiencies of each component in the system whose values are provided by the manufacturers. Alternatively, a calibrated light source is injected into the system to obtain the measured transmission intensity which is given by : $\epsilon(\lambda) = N_{\lambda}^{cal}/N_{\lambda}^{th}$, where is the N_{λ}^{cal} is the measured light spectrum and N_{λ}^{th} is the theoretical transmission spectrum by the manufacturer. The light source used was the tungsten -halogen light source [12]. Fig. 6 (left) shows the modelled and measured transmission intensity curves. Fig. 6 (right) shows the calculated systematic uncertainty in the measurements. It is obtained from the relative error between the two curves.

A.2 Cosmic ray background suppression

Fig.7 (left) shows the example of SiPM photon emission recorded in spectroscopy mode in PI camera with traces of cosmic rays shown in grey. Fig.7 (right) instead shows the SPAD photon emission after cosmic ray background suppression algorithm was applied.

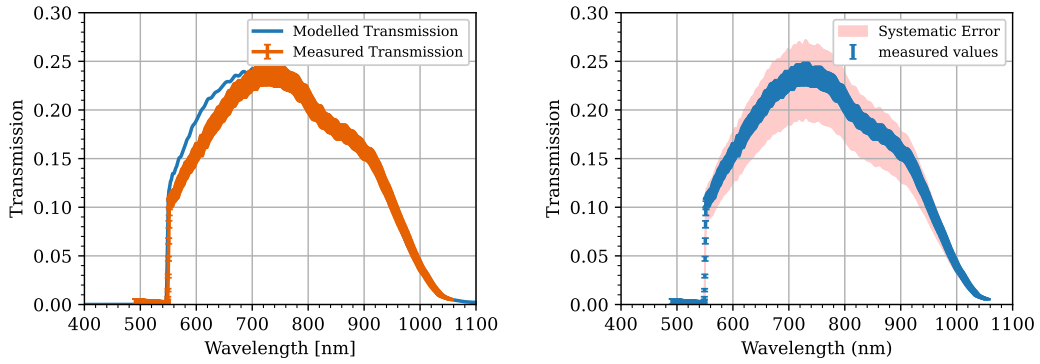


Figure 6: **Left:** Modelled transmission is obtained from the resultant product of all individual transmission curves of optical components in the system. The measured transmission curve is obtained using a calibrated tungsten-halogen light source. **Right:** The systematic uncertainty on the measurements.

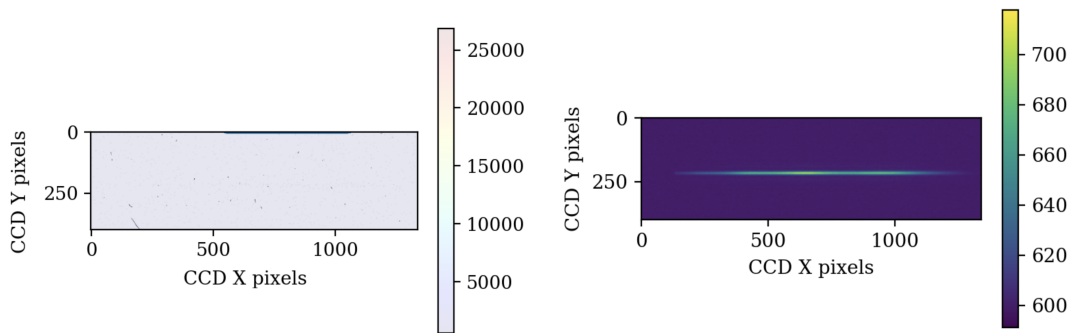


Figure 7: **Left:** Spectroscopy image of the SiPM captured with prominent cosmic interactions. The SPAD light emission is completely suppressed. **Right:** Spectroscopy image with cosmic ray background suppression implemented. The SPAD light emission is clearly visible.